Crossover from integer to fractional quantum Hall effect

Koji Kudo,[1,2] Jonathan Schirmer,[1,3] and Jainendra K. Jain[1]
[1]*Department of Physics, The Pennsylvania State University, University Park, Pennsylvania 16802, USA*
[2]*Department of Physics, Kyushu University, Fukuoka 819-0395, Japan*
[3]*Department of Physics, William & Mary, Williamsburg, Virginia 23187, USA*

(Received 13 November 2023; revised 22 January 2024; accepted 6 February 2024; published 26 February 2024; corrected 5 September 2024)

The parton theory constructs candidate fractional quantum Hall states by decomposing the physical particles into unphysical partons, placing the partons in integer quantum Hall states, and then gluing the partons back into the physical particles. Field theoretical formulations execute the gluing process through the device of emergent gauge fields. Here we study numerically the process of going from the integer quantum Hall effect of two species of fermionic partons to the fractional quantum Hall effect of bosons by introducing an attractive interaction between the fermions of different species and continuously increasing its strength to glue them into bosons. To properly capture the physics in the bulk, we implement this process in a lattice version of the spherical geometry, which allows us to keep the full Hilbert space. Even though the two end-point states are topologically distinct, we find that, for the small system sizes accessible to our study, the energy gap remains open, indicating a crossover between these two states.

DOI: 10.1103/PhysRevB.109.075157

I. INTRODUCTION

The integer and the fractional quantum Hall effects [1,2] are the prototypical examples of topological phases of matter, characterized by the Chern number [3–5]. They are fundamentally distinct in many important ways. The integer quantum Hall effect (IQHE) is a property of noninteracting electrons, whereas the fractional quantum Hall effect (FQHE) occurs due to the interaction between electrons. Furthermore, the IQHE state has fermionic excitations, whereas the excitations of the FQHE have fractional charge and fractional statistics [6–9]. For these reasons, one would a priori not expect there to be any way to connect these phenomena adiabatically.

The composite fermion (CF) theory [10,11] revealed a unified underlying description in which the FQHE at the fractions $\nu = n/(2pn \pm 1)$ with p, n integers, is explained as the $\nu = n$ IQHE of CFs binding $2p$ flux quanta. This inspired ingenious ideas that demonstrate adiabatic continuity between the IQHE and the FQHE by trading external magnetic flux for statistical flux in such a fashion that the intermediate anyon system always maps into the IQHE system in a mean field sense [12–19].

In this paper, we propose and demonstrate for small systems accessible to numerical studies, adiabatic continuity between the IQHE and the FQHE through a different route. This is inspired by the parton construction of the FQHE [20,21], which provides another paradigm for the understanding of the FQHE in terms of IQHE. In the parton construction, each electron is divided into m species of fictitious fermionic particles called partons. Because of the Fermi statistics of electrons, m must be an odd integer. One places each species of partons in the IQHE state Φ_{n_λ} with filling n_λ $(\lambda = 1, \ldots, m)$ to produce $\prod_{\lambda=1}^{m} \Phi_{n_\lambda}(\{z_j^{(\lambda)}\})$, which will be referred to as the $(n_1, n_2, \ldots)$ state. One finally glues the partons back together (i.e., sets $z_j^{(\lambda)} = z_j$) to recover electrons in an incompressible state. The resulting wave function

$$\Psi_\nu(\{z_j\}) = \prod_{\lambda=1}^{m} \Phi_{n_\lambda}(\{z_j\}) \tag{1}$$

yields a state at filling factor $\nu = (\sum_\lambda n_\lambda^{-1})^{-1}$. (More generally, one can take partons to be either bosons or fermions, and place them in any known incompressible states.) This construction provides a large class of candidate FQHE states, which include not only the previous Jain CF states but also many new states some of which support non-Abelian excitations [22]; many of these new states have been shown to be plausible for several observed FQHE states that are not explicable in terms of noninteracting CFs [23–31]. The subject of our article is to follow the parton construction to seek a new scheme for connecting IQHE to FQHE in an adiabatic fashion.

Let us illustrate the issue by taking the simple example of the 1/2 bosonic FQHE. We first divide each boson into two fermionic partons and place each species in $\nu = 1$ state, obtaining the (1,1) state

$$\begin{aligned}\Psi_{(1,1)}(\{z_j\}, \{w_j\}) &= \Phi_1(\{z_j\})\Phi_1(\{w_j\}) \\ &= \prod_{i<j=1}^{N} (z_i - z_j) \prod_{i<j=1}^{N} (w_i - w_j),\end{aligned} \tag{2}$$

where $z_j = x_j - iy_j$ and $w_j = x_j - iy_j$ are the positions of the two parton species. The ubiquitous Gaussian factor is suppressed for simplicity. Next, we introduce an attractive contact interaction $-U \sum_{ij} \delta^2(z_i - w_j)$ between the different species with $U > 0$ and increase the value of U from 0 to ∞ to glue partons together to form bosons. The Pauli principle of the partons results in a short-range repulsion between the

bosons. Since the filling factor is $1/2$ for bosons, the "final" ground state in the strong interaction limit is expected to be the Laughlin-like state:

$$A\prod_j \delta^2(v_j)\prod_{i<j}(V_i - V_j)^2 = A\prod_j \delta^2(v_j)\Psi_{1/2}(\{V_j\}), \quad (3)$$

where $v_j = z_j - w_j$, $V_j = (z_j + w_j)/2$, $\Psi_{1/2}$ is the bosonic Laughlin state at filling factor $1/2$, and A represents antisymmetrization with respect to all fermions within one species.

The initial and the final states, i.e., (1,1) and $1/2$, appear drastically different. First, while the initial (1,1) state resides in the lowest Landau level (LLL) of the partons, the final $1/2$ state involves all Landau levels (LLs) of the partons because of the delta function; i.e., the LLs of partons must strongly mix to form bosons and their LLs. Second, the initial and final states are topologically distinct. While the former has fermionic excitations, the latter has anyonic excitations. [We note that the charge of both excitations is one, but for fundamentally different reasons. For (1,1) it is simply a charge one fermion, whereas for the $1/2$ state it is a fractionally charged excitation of charge-two bosons.] For these reasons, one might expect the gap to close at some point as we go from the (1,1) fermionic state to the $1/2$ bosonic state.

We nonetheless address this question by numerical diagonalization. Such studies have been very useful in clarifying the physics of the FQHE, as well as for confirming the validity of various concepts. A numerical study of the present problem faces two major hurdles. First is the absence of an energy cutoff, which requires one to include *all* LLs of the partons. Second, the method of the standard Haldane pseudopotentials [7] also is not applicable here, as all LLs must be included in the calculation.

We circumvent these problems by working on a lattice version of the spherical geometry, namely a subdivided icosahedron lattice, which has a finite Hilbert space. Many numerical studies of the FQHE have made use of the spherical geometry. We formulate a gauge convention to realize a uniform magnetic field on the subdivided icosahedron lattice. Using this setting, we numerically show that, at least for finite systems that we could study, the IQHE states of the partons are adiabatically connected, without any gap closing, to the bosonic FQHE states as we increase the strength of the attractive interaction.

The idea of going from a two-component integer quantum Hall state to a one component bosonic FQHE has been considered in the past [32–35]. Repellin *et al.* have studied the problem on a lattice in the torus geometry and they find that the ground state becomes doubly degenerate at some value of the interaction, as expected given that the $1/2$ FQHE state is doubly degenerate on torus; they also identify a phase transition by considering the entanglement spectrum [34]. Yang and Zhai have derived the effective field theory of the quantum phase transition [32].

In the spherical geometry (a subdivided icosahedron lattice) used for our calculations, all incompressible FQHE states are nondegenerate. Also, the two terminal states, for example the (1,1) and the $1/2$ states, occur at the same shift in the spherical geometry. The absence of a gap closing may seem inconsistent with the fact that the nature of the low-energy excitations changes qualitatively, from fermionic to anyonic, in the two limits. (Note that the fractional charge and statistics of the quasiparticle excitations can be defined for fairly small systems for the bosonic Laughlin $1/2$ state [36,37].) However, there exist other examples where the excitations change their character qualitatively even though the gap does not close (for small systems), such as the transition between the Jain and the Gaffnian states at $\nu = 2/5$ [38–40] and the crossover between the BCS to the BEC state where the low-energy excitations go from broken pairs to density waves.

For completeness, we also study this problem in the torus geometry, where a FQHE state is known to have degeneracies due to translation symmetry (and, additional degeneracies for non-Abelian states). Our results are consistent with those of Ref. [34]. In a previous work studying an adiabatic process through anyons, the dimension of the Hilbert space changes discretely due to algebraic constraints of the braid group [41,42], resulting in a peculiar structure in the adiabatic evolution: the ground state degeneracy changes wildly even though the energy gap varies smoothly [14]. This may be understood from the fact that apart from the degeneracy, the states have the same underlying topology. For our present case, we find that the IQHE state of partons evolves into one of the degenerate FQHE ground states of the physical particles, while other states approach it to produce the required degeneracy for the ground state in the $U = \infty$ limit. These additional states carry a nontrivial many-body Chern number, and the collection of degenerate states exhibits the same Hall conductance as the IQHE state of partons.

While our model is motivated by the parton theory of the FQHE, it is interesting to ask if it can be realized by considering systems where the partons are real (as opposed to fictitious) fermions. In principle, it applies to a system of spin-up and spin-down electrons each at an integral filling. In the limit when the electrons are noninteracting, both the up and down spin electrons fill an integer number of LLs, which is the case at even integer fillings in typical experiments. In the other limit with a strong onsite attraction, they exhibit a FQHE state of bosonic bound states consisting of two electrons. Achieving a strong attractive interaction between spin-up and spin-down electrons appears unrealistic, however. The same is true for a system of fermions in two layers. A more promising platform is ultracold atomic systems. One can, in principle, achieve FQHE states in cold atom systems by creating a synthetic magnetic field through either rotation or complex hopping phases. We refer the reader to Ref. [43] for recent progress as well as for references to the earlier literature. One can thus imagine starting with the IQHE states of two species of noninteracting fermions (which could be the same fermionic atoms but in different internal states). By tuning through the Feshbach resonance it is possible to make the short range interaction between the different species of fermions dominant and attractive. Our study suggests that as the strength of the attractive interaction is enhanced, the system with a finite number of particles will evolve, without gap closing, into a FQHE state of bosonic molecules. This is therefore a possible way to generate bosonic FQHE states in cold atom systems. The physics here is reminiscent of the BCS to BEC crossover [44,45], which has been realized in

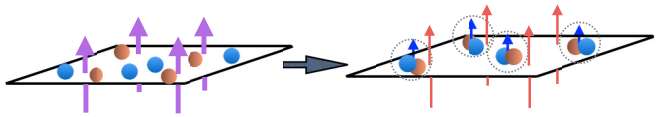

FIG. 1. A schematic depiction of the crossover from the IQHE of two species of fermions to the FQHE of their bosonic molecules. The left panel shows two species of fermions, red and blue, each at filling factor one. Each thick arrow represents a flux of magnitude h/e. As the inter-species attractive interaction is dialed up, the fermions form charge-$2e$ bosonic molecules at filling factor $1/2$, because now there are twice as many $h/2e$ flux quanta. The bosonic molecules capture a single $h/2e$ flux quantum each (represented by a thin arrow) to become composite fermions at filling factor one, thereby forming an incompressible FQHE state.

ultracold Fermi gases [46–48]. Figure 1 illustrates the physics pictorially.

II. ICOSAHEDRON WITH A MAGNETIC MONOPOLE

The spherical geometry [7], which considers N electrons moving on the surface of a sphere subjected to a radial magnetic field produced by an enclosed magnetic monopole, is very convenient for the study of the FQHE. As noted in the introduction, this geometry is not suitable for the problem at hand, which requires a consideration of arbitrarily high LLs. To circumvent this issue, we begin by constructing a lattice analog of the quantum Hall problem in the spherical geometry [7,49,50]. We choose a regular icosahedron because it is the Platonic solid with the most faces [51] resembling a sphere. This similarity is expected to result in a better representation of a continuous sphere than that provided by other polygons.

We subdivide each triangle into four new equilateral triangles and repeat the process n times [52]. We call the resulting figure an n-icosahedron. Figure 2(a) shows illustrations with $n = 0,\ 1,$ and 2. As mentioned below, this subdivision structure proves helpful for assigning the Peierls phases that describe the magnetic field. The numbers of faces, edges, and vertices of an n-icosahedron, denoted by F_n, E_n, and V_n, respectively, satisfy the recurrence relations $F_{n+1} = 4F_n$, $E_{n+1} = 2E_n + 3F_n$, and $V_{n+1} = V_n + E_n$. Using $(F_0, E_0, V_0) = (20, 30, 12)$, we have

$$(F_n, E_n, V_n) = (20 \times 4^n, 30 \times 4^n, 10 \times 4^n + 2). \quad (4)$$

As a sanity check, one can verify the Euler's polyhedron formula $V_n - E_n + F_n = 2$ for any n.

The tight-binding Hamiltonian for an n-icosahedron is given by

$$H = -t \sum_{\langle ij \rangle} e^{\mathrm{i}\alpha_{ij}} \hat{c}_i^\dagger \hat{c}_j, \quad (5)$$

where $\hat{c}_i^\dagger$ is the creation operator for a fermion on site i and $\langle ij \rangle$ indicates summation over all nearest neighbors. The Peierls phases α_{ij} are chosen to produce a radial magnetic field. For a 0-icosahedron (namely icosahedron), one can easily assign α_{ij} by using the string gauge [53]. In Fig. 2(b), we show the unwrapped net of the icosahedron with the gauge convention. Here, we select one triangle as the "root" triangle, and draw strings starting from this triangle to all other triangles called "normal" triangles. Then, we set $\phi_{ij} = 2\pi\phi n_{ij}$,

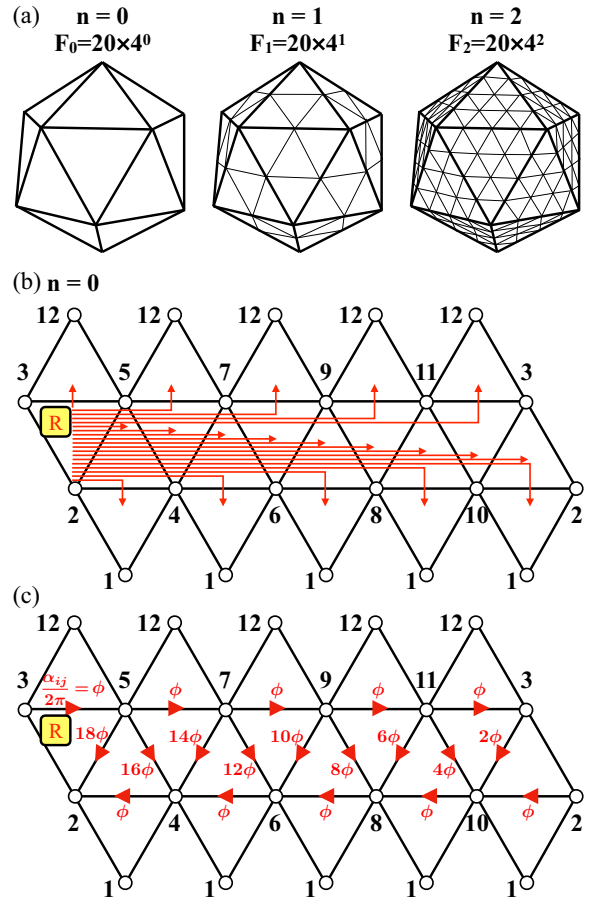

FIG. 2. (a) n-icosahedron with $n = 0,\ 1,$ and 2. F_n is the number of (smallest) triangles. (b) The unwrapped "net" of a 0-icosahedron, i.e., an icosahedron. Each site is labeled. Strings emanate from the root triangle, indicated by the "R" and terminate at each of the other (normal) triangles. (c) The Peierls phases $\alpha_{ij} = 2\pi\phi n_{ij}$, where n_{ij} is the number of strings that cross the bond ij. The direction of the arrow is toward right as we cross any edge. The total flux through any closed loop (in units of the flux quantum) is the sum of phases for a traversal along that loop in the counterclockwise direction. Fluxes of -19ϕ and ϕ pass through the root triangle and each of the normal triangles, respectively.

where n_{ij} is the number of strings that cross the bond ij as shown in Fig. 2(c), and ϕ is the flux through a single triangle in units of the flux quantum $\phi_0 = hc/e$ (we will see that ϕ takes fractional values). This encodes a flux of $(1 - F_0)\phi$ through the root triangle and ϕ through all other normal triangles. A uniform magnetic field is obtained if $e^{-i2\pi(1-F_0)\phi} = e^{i2\pi\phi}$, i.e., $\phi = N_\phi/F_0$ with $N_\phi = 0, 1, \ldots, F_0 - 1 = 19$. Note that N_ϕ corresponds to the total magnetic fluxes in units of ϕ_0 and is always an integer, consistent with the Dirac quantization condition.

For an n-icosahedron with $n > 0$, it is technically harder to place strings and systematically assign α_{ij}. We instead employ an inductive approach. Assume that we have α_{ij} for an n-icosahedron, where a flux of $-(F_n - 1)\phi_n$ passes through a root triangle, and a flux ϕ_n passes through each of the $F_n - 1$ normal triangles. This is satisfied in the case of $n = 0$ discussed above. When subdividing each triangle to four parts for an $n + 1$-icosahedron, we define a new set of α_{ij} as shown

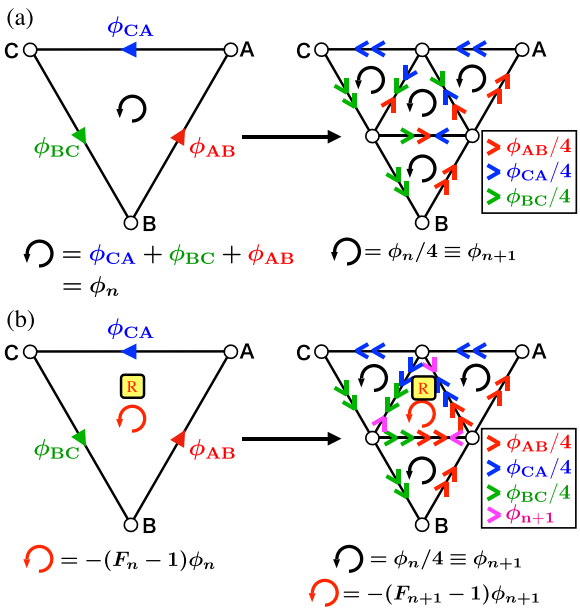

FIG. 3. This figure shows how a triangle ABC can be subdivided into four equilateral triangles such that the magnetic flux through each is equal. (a) A flux of ϕ_n in a normal triangle is divided into four equal units of $\phi_{n+1} = \phi_n/4$ through the convention shown. The value of the phase associated with each arrow on the figure on the right is shown in the box. (b) This shows the Peierls phases for the root triangle after subdivision. A flux of $-(F_n - 1)\phi_n$ in the root triangle is divided into three fluxes of $\phi_n/4$ and one of $-(F_{n+1} - 1)\phi_{n+1}$.

in Fig. 3(a) for a normal triangle and in Fig. 3(b) for the root triangle. We can simultaneously perform this subdivision for all triangles. In the resulting $n+1$-icosahedron, a flux of $\phi_{n+1} \equiv \phi_n/4$ passes through each of the $F_{n+1} - 1$ normal triangles while a flux of $-(F_{n+1} - 1)\phi_{n+1}$ passes through the root triangle. Starting from the string gauge at $n = 0$, an iteration of this procedure systematically produces α_{ij} for an n-icosahedron.

Now, we use the symbol ϕ instead of ϕ_n for simplicity for the flux through a single triangle of an n-icosahedron. The condition for the uniform magnetic field is

$$e^{-i2\pi(F_n-1)\phi} = e^{i2\pi\phi}, \tag{6}$$

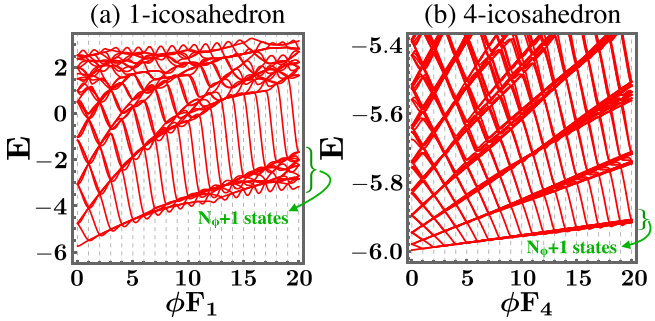

FIG. 4. Single-particle energies for (a)1-icosahedron and (b) 4-icosahedron. The energy E is measured in units of t. The dashed lines represent $\phi F_n =$ integer in which the magnetic filed is uniform and the total flux is given by $N_\phi = \phi F_n$. The $N_\phi + 1$ lowest energy states form a lattice analog of the LLL on a sphere.

i.e., $\phi = N_\phi/F_n$ with $N_\phi = 0, 1, \ldots, F_n - 1$. In Fig. 4(a), we plot the single-particle energies as functions of ϕF_1 for a 1-icosahedron. If ϕF_1 is a small integer ($\lesssim 7$), the lowest energy states form a multiplet of $(\phi F_1 + 1)$ exactly or nearly degenerate states. This is consistent with the degeneracy of the lowest Landau level (LLL) on a sphere. (The exact degeneracy comes from some symmetry of an icosahedron [50].) As ϕ increases, the energy splitting within the multiplet becomes larger due to the effect of the lattice. Figure 4(b) shows the energy spectrum for a 4-icosahedron. The numbers of faces and sites are much larger than those of a 1-icosahedron and, therefore, the effect of the lattice is suppressed and nearly degenerates states associated with the LLL on a sphere are observed in a wide range of integer ϕF_4. These results demonstrate the validity of our lattice discretization of the spherical geometry.

III. HUBBARD HAMILTONIAN FOR PARTONS

Let us come to the many-body problem. The main purpose here is to investigate the transition between two quantum Hall states associated with the parton construction: a tensor product of IQHE states of two species of partons and a FQHE state of bosons that are bound states of two partons.

To this end, we consider a system of two-component lattice fermions (partons) in a magnetic field, with an attractive on-site interaction (because of the Pauli principle, this implies attraction only between partons of different species). By labeling the species by spin our problem reduces to the standard Hubbard model of spin 1/2 particles as

$$H = -t \sum_{\langle ij \rangle} \sum_{\sigma=\uparrow,\downarrow} \hat{c}^\dagger_{i\sigma} e^{i\alpha_{ij\sigma}} \hat{c}_{j\sigma} - U \sum_i \hat{n}_{i\uparrow}\hat{n}_{i\downarrow}, \tag{7}$$

in a magnetic field. Here $\hat{c}^\dagger_{i\sigma}$ is the creation operator for a fermion on site i with spin σ, and we define $\hat{n}_{i\sigma} = \hat{c}^\dagger_{i\sigma}\hat{c}_{i\sigma}$. The charge depends on the spin, denoted by $e_\uparrow$ and $e_\downarrow$, which implies the relation $\alpha_{ij\uparrow}/\alpha_{ij\downarrow} = e_\uparrow/e_\downarrow$.

As mentioned previously, we arrange parameters such that the state at $U = 0$ is an IQHE state $(n_\uparrow, n_\downarrow)$ and the state for $U \to \infty$ is a FQHE state at $\frac{n_\uparrow n_\downarrow}{n_\uparrow + n_\downarrow}$. The intermediate state will be labeled $(n_\uparrow, n_\downarrow; \frac{n_\uparrow n_\downarrow}{n_\uparrow + n_\downarrow})$.

Now, we specialize to a balanced configuration with $N_\uparrow = N_\downarrow \equiv N$. The system at $U = 0$ is decomposed into two spin parts, with the integer filling factor $n_{\sigma=\uparrow,\downarrow}$ and the "shift" S_σ related by

$$N_{\phi_\sigma} = \frac{N}{n_\sigma} - S_\sigma, \tag{8}$$

where N_{ϕ_σ} is the number of fluxes in units of $\phi_\sigma = h/e_\sigma$. The shift on a sphere (torus) is given by $S_\sigma = n_\sigma$ (0). At $U/t = +\infty$, on the other hand, the ground state is macroscopically degenerate, where all sites are either doubly occupied or empty. As derived in Appendix, this degeneracy is lifted at any finite but large U where the effective Hamiltonian in the second-order perturbation theory is given by

$$H_{\text{eff}} = -\beta \sum_{\langle ij \rangle} \hat{b}^\dagger_i e^{i(\alpha^\uparrow_{ij} + \alpha^\downarrow_{ij})} \hat{b}_j - \beta \sum_j s_j \hat{n}_j + 2\beta \sum_{\langle ij \rangle} \hat{n}_i \hat{n}_j. \tag{9}$$

Here, $\beta = 2t^2/U$, $\hat{b}_j^\dagger$ is the creation operator of a hard-core boson on site j, $\hat{n}_j = \hat{b}_j^\dagger \hat{b}_j$, and s_j is the coordination number of site j. The hard-core repulsion comes from the Pauli principle of the partons, which prevents two bosons from occupying the same site. The filling factor ν_b and the shift S_b for these bosons are defined by

$$N_{\phi_\mathrm{b}} = \frac{N}{\nu_\mathrm{b}} - S_\mathrm{b}, \tag{10}$$

where N_{ϕ_b} is the number of fluxes in units of $\phi_\mathrm{b} = h/e_\mathrm{b}$ with $e_\mathrm{b} = e_\uparrow + e_\downarrow$. The numbers of fluxes for each particle satisfy

$$N_{\phi_\uparrow} + N_{\phi_\downarrow} = N_{\phi_\mathrm{b}}. \tag{11}$$

This relation reduces to

$$\nu_\mathrm{b} = \frac{n_\uparrow n_\downarrow}{n_\uparrow + n_\downarrow}, \tag{12}$$

$$S_\mathrm{b} = S_\uparrow + S_\downarrow. \tag{13}$$

We investigate adiabatic continuity between the $(n_\uparrow, n_\downarrow)$ state and the $\frac{n_\uparrow n_\downarrow}{n_\uparrow + n_\downarrow}$ state via exact diagonalization as we vary U from 0 to a sufficiently large number. This article focuses on basic examples where $(n_\uparrow, n_\downarrow; \frac{n_\uparrow n_\downarrow}{n_\uparrow + n_\downarrow}) = (1, s; \frac{s}{1+s})$ with s integer. The simplest case is $(1, 1; 1/2)$, which interpolates between the (1,1) and $1/2$ states as U is increased from 0 to $U/t \gg 1$. (Due to the contact interaction, the ground state of H_eff at $\nu_b = 1/2$ is the lattice analog of the Laughlin state.) Systems on an 1-icosahedron or on a torus are considered below. We will also consider the case of $(n_\uparrow, n_\downarrow; \frac{n_\uparrow n_\downarrow}{n_\uparrow + n_\downarrow}) = (1, 2; 2/3)$ and $(1, 3; 3/4)$ in the torus geometry. (We cannot access these systems on a 1-icosahedron. For the (1,2) state, say, we must have a minimum of $2N = 8$ particles because it takes a minimum of four particles to fill the two LLs. The dimension of the Hilbert space for this system is 12 528 324 900 which is too large to perform exact diagonalization with computer resources currently available.) For exact diagonalization, we use the Lanczos method [54].

IV. NUMERICAL DIAGONALIZATION

A. 1-icosahedron

We begin with two species of fermions on a 1-icosahedron. Figure 5(a) shows the energy spectrum for $(n_\uparrow, n_\downarrow; \frac{n_\uparrow n_\downarrow}{n_\uparrow + n_\downarrow}) = (1, 1, 1/2)$ for a system of $2N = 4$ fermions. (We measure all energies relative to the energy of the ground state.) As mentioned above, the (1,1) ground state at $U = 0$ is the tensor product of two IQHE states. The increase of U from 0 leads to reconstruction of the single-particle spectrum from fermionic to bosonic LLs, which results in many level crossings as shown in the figure. However, the ground state adiabatically evolves as U is varied without any gap closing. While Fig. 5(a) shows the gap in the range of $U/t \in [0, 20]$ (we quote energies in units of t), its inset plots the gap with $U/t \in [20, \infty)$ as a function of t/U. As t/U decreases, the gap remains open in units of $\beta = 2t^2/U$ and approaches the energy gap of the $\nu_\mathrm{b} = 1/2$ Laughlin state computed by diagonalizing the effective Hamiltonian H_eff in Eq. (9). In Fig. 5(c), we show results for a system of $2N = 6$ fermions. Due to large matrices, we plot only a few lowest energy states. Again, the energy gap of the (1,1) state monotonically decreases and approaches the

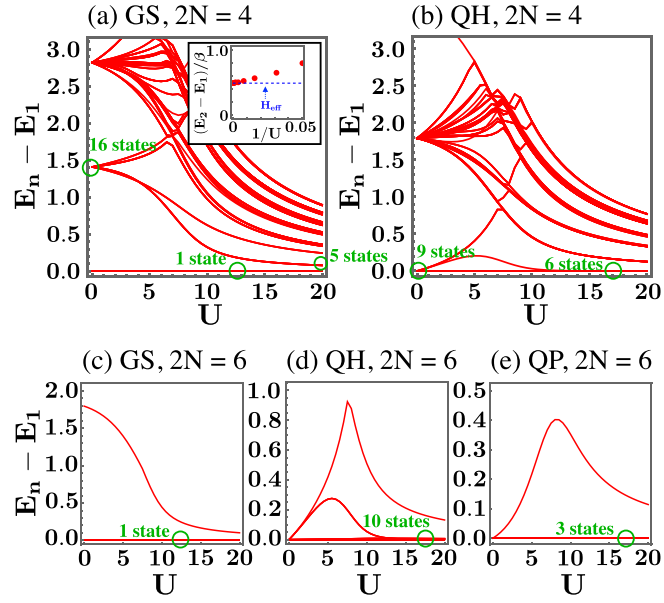

FIG. 5. Many-body energy at $(n_\uparrow, n_\downarrow; \frac{n_\uparrow n_\downarrow}{n_\uparrow + n_\downarrow}) = (1, 1; 1/2)$ on a 1-icosahedron. We set $t = 1$. GS/QH/QP represent ground state, quasihole state, and quasiparticle state. $2N$ is the total particle number ($N_\uparrow = N_\downarrow \equiv N$). The number of magnetic fluxes is (a) $N_{\phi_\uparrow} = 1$, (b) 2, (c) 2, (d) 3, and (e) 1. We plot the lowest N_cut energies at each U with [(a) and (b)] $N_\mathrm{cut} = 100$, (c) 2, (d) 11, and (e) 4. The inset in (a) shows the gap for the first-excited state scaled by $\beta = 2/U$ as a function of $1/U$. The blue dashed line indicates the value computed by using H_eff.

value estimated by the $\nu_\mathrm{b} = 1/2$ Laughlin state as U increases. These results demonstrate adiabatic continuity between the (1,1) state of partons and the bosonic $1/2$ Laughlin state for systems with 4 and 6 fermions. A study of larger systems is not possible due to the very large dimension of the Fock space (the dimension is 12 528 324 900 for $2N = 8$ particles).

Next, we consider elementary excitations, beginning with the neutral excitation. The first excited states at $U = 0$ and $U = 20$ in Fig. 5(a), which are associated with an exciton, are not adiabatically connected. In fact, they have different counting: there is 16-fold degeneracy at $U = 0$ while fivefold degeneracy at $U = 20$. (Hereafter, we consider two states to be degenerate if their energy difference, scaled by t or β in the weak or strong interaction regime, is less than 0.1. One can ascertain the extent of the degeneracy by referring to figures.) These degeneracies are in agreement with the known degeneracies for the continuum sphere. For the (1,1) state, we have two copies of one filled LL of two fermions. The monopole strength is $Q = 1/2$, and thus the angular momenta of the excited fermion is $3/2$ and the hole is $1/2$. These produce $3/2 \otimes 1/2 = 1 \oplus 2$, giving a total of eight states for each species of fermions, producing a degeneracy of 16. In the large U limit, we have the two particle bosonic $1/2$ state, which maps into the 2 particle $\nu = 1$ state of CFs. This again produces $3/2 \otimes 1/2 = 1 \oplus 2$, but the $L = 1$ is known to be annihilated by LLL projection [55], producing a total of 5 states. The absence of adiabatic continuity reflects the qualitatively different characters of the excitations in the two limits: quasiholes/quasiparticles of the (1,1) and the $\nu_\mathrm{b} = 1/2$

Laughlin states obey different statistics, namely fermionic and semionic, respectively. It is interesting to note that in both limits the charge of the elementary excitation is the same, but for the (1,1) state it is simply an excited fermion, whereas for the bosonic 1/2 state, it is a charge 1 Laughlin quasihole in the 1/2 state of charge-2 bosons.

Figures 5(b) and 5(d) show the spectrum for systems with one additional flux for each species (or two additional fluxes for the bosonic system). These are the quasihole states. Again, there is no adiabatic continuity, as expected. For Fig. 5(b) there is a ninefold degeneracy at $U = 0$ while a sixfold degeneracy at $U = 20$. The degeneracies in the two limits are consistent with the known degeneracies on sphere. For example, for the $2N = 4$ particle system: the angular momentum of each quasihole for the (1,1) state is 1, producing $L = 1 \otimes 1 = 0 \oplus 1 \oplus 2$, and for the 1/2 Laughlin state with two quasiholes, we have $L = 0 \oplus 2$. Figure 5(e) plots the spectrum for quasiparticle states of $2N = 6$ fermions. The obtained degeneracies at $U = 20$ in Fig. 5(e) are consistent with the corresponding degeneracies on sphere.

B. Torus

As discussed above, in the torus geometry the $(n_\uparrow, n_\downarrow) = (1, s)$ state with s integer is nondegenerate, whereas the $\frac{n_\uparrow n_\downarrow}{n_\uparrow + n_\downarrow} = \frac{s}{1+s}$ state has $(1 + s)$-fold degeneracy coming from translation symmetry. In this section we investigate the evolution of the system in the torus geometry as a function of U.

We consider a square lattice with $N_x \times N_y = 6 \times 6$ sites. Periodic boundary conditions are imposed in both directions unless otherwise stated. In Figs. 6(a)–6(c), the evolution of the lowest few eigenstates are shown for $(n_\uparrow, n_\downarrow; \frac{n_\uparrow n_\downarrow}{n_\uparrow + n_\downarrow}) = (1, 1; 1/2)$, $(1, 2; 2/3)$ and $(1, 3; 3/4)$. While the ground state is nondegenerate for small U, it has a degeneracy of 2, 3, and 4, respectively, at large U. The inset of Fig. 6(a) shows that, as t/U decreases, the gap for the second-excited state scaled by $\beta = 2t^2/U$ approaches to the value estimated by diagonalizing H_{eff}. These results are consistent with those of Ref. [34].

To investigate the topological structures of states, we calculate the many-body Chern number C, which is the sum of the Chern numbers of the eigenstates that we associate with the ground state multiplet (or an excited state multiplet) on the torus. It is given by [5]

$$C = \frac{1}{2\pi i} \int_{T^2} d^2\eta F, \tag{14}$$

$$F = \frac{\partial A_y}{\partial \eta_x} - \frac{\partial A_x}{\partial \eta_y}, \tag{15}$$

$$A_{x(y)} = \mathrm{Tr}\left[\Phi^\dagger \frac{\partial \Phi}{\partial \eta_{x(y)}}\right], \tag{16}$$

where $T^2 = [0, 2\pi] \times [0, 2\pi]$, $\Phi = (|\Phi_j\rangle, |\Phi_{j+1}\rangle, \ldots, |\Phi_{j+n}\rangle)$, $|\Phi_j\rangle$ is the jth lowest energy state, and $\vec{\eta} = (\eta_x, \eta_y)$ are the twist angles defined as

$$\hat{c}^\dagger_{N_x+i_x,i_y,\sigma} = e^{i\eta_x} \hat{c}^\dagger_{i_x,i_y,\sigma}, \tag{17}$$

$$\hat{c}^\dagger_{i_x,N_y+i_y,\sigma} = e^{i\eta_y} \hat{c}^\dagger_{i_x,i_y,\sigma}. \tag{18}$$

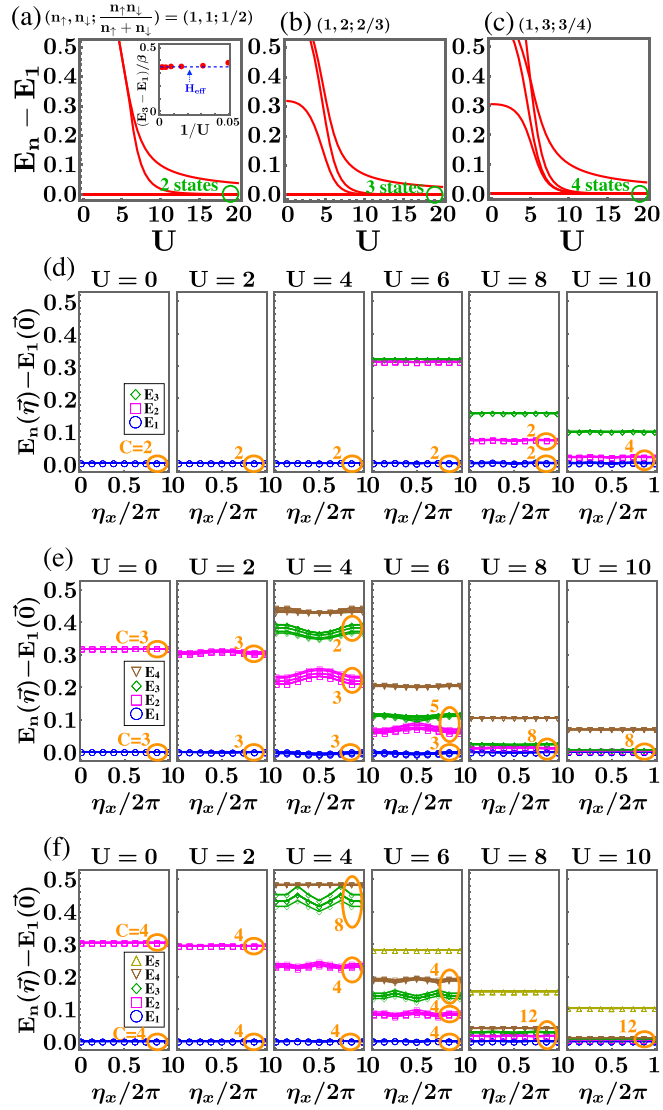

FIG. 6. [(a)–(c)] Many-body energy on a torus at $(n_\uparrow, n_\downarrow; \frac{n_\uparrow n_\downarrow}{n_\uparrow+n_\downarrow}) = (1, s; \frac{s}{s+1})$ with (a) $s = 1$, (b) 2, and (c) 3. We quote energies in units of t. The total particle number is [(a) and (c)] $2N = 6$ and (b) 4. We plot the lowest N_{cut} energies with (a) $N_{\text{cut}} = 3$, (b) 4, and (c) 5. The inset in (a) shows the gap $(E_3 - E_1)/\beta$ with $\beta = 2/U$ as a function of $1/U$. The blue line indicates the value computed by using H_{eff}. [(d)–(f)] Spectral flows for the systems considered in [(a)–(c)] as functions of η_x. We set $\eta_y = 2\pi n_y/8$ with $n_y = 0, 1, \ldots, 7$. The color expresses "n" of E_n. The numbers in orange are the many-body Chern number C of the circled states.

For numerical calculation, we compute the discretized local Berry curvature $\mathcal{F}$ using the method in Ref. [56]. Figures 6(d)–6(f) show the spectral flows at several U for the system considered in Figs. 6(a)–6(c), respectively. The parameters in Figs. 6(d)–6(f) are $(n_\uparrow, n_\downarrow; \frac{n_\uparrow n_\downarrow}{n_\uparrow+n_\downarrow}) = (1, s; \frac{s}{1+s})$ with $s = 1$, 2, and 3, respectively. The energy in Fig. 6(d) is insensitive to the twist angles $\vec{\eta}$, which is consistent with a property of a gapped phase [57]. (As shown in Fig. 7, the Berry curvature is also nearly flat. This is consistent with the expected behavior of the quantum Hall systems [57–61].) The unique ground state at $U = 0$ in the figures carries $C = 1 + s$,

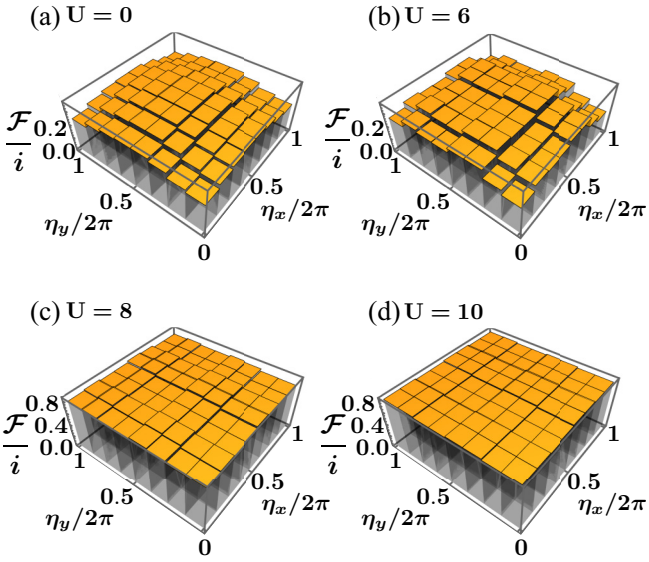

FIG. 7. Discretized local Berry curvature $\mathcal{F}/i$ for the system considered in Fig. 6(e). The Berry curvature is defined with the M lowest energy states with [(a) and (b)] $M = 1$ and [(c) and (d)] 3. The Chern number is given by summing $\mathcal{F}$ over all mesh points.

consistent with the Hall conductance of

$$\sigma_{xy} = \frac{e_\uparrow^2}{h} + s\frac{e_\downarrow^2}{h}. \tag{19}$$

As U increases, some states with the nontrivial Chern number go down and eventually the $1+s$-fold degenerate ground state with $C = 4s$ is observed at $U = 20$. Since the boundary conditions for H_{eff} are given by $(\eta_x^{\text{eff}}, \eta_y^{\text{eff}}) = (2\eta_x, 2\eta_y)$, the Hall conductance with respect to bosons is

$$\sigma_{xy} = \frac{C_{\text{eff}}}{1+s}\frac{e_{\text{b}}^2}{h} = \frac{s}{1+s}\frac{e_{\text{b}}^2}{h}, \tag{20}$$

where $C_{\text{eff}} = C/2^2$ corresponds to the Chern number integrating over $(\eta_x^{\text{eff}}, \eta_y^{\text{eff}})$ instead of (η_x, η_y). Using $e_{\text{b}} = e_\uparrow + e_\downarrow$ and $e_\uparrow/e_\downarrow = n_\downarrow/n_\uparrow = s$, one can show $\frac{s}{1+s}\frac{e_{\text{b}}^2}{h} = \frac{e_\uparrow^2}{h} + s\frac{e_\downarrow^2}{h}$. This implies that the quantum Hall states at $U = 0$ and $U = 20$ exhibit the same Hall conductance, despite having different Chern numbers.

V. CONCLUDING REMARKS

In this paper, we have developed an adiabatic scheme connecting IQHE and FQHE for systems with a finite number of particles, motivated by the parton construction of the FQHE. Specifically, we begin with an IQHE state of two species of fermionic partons and vary the attractive onsite interaction between partons from 0 to ∞ so they produce a FQHE state of bosonic bound states of partons. Because this involves a drastic reorganization of the states, it is necessary to include the full Hilbert space, and therefore we consider particles moving on a lattice. We consider both the spherical geometry, where the lattice is a subdivided icosahedron, and the torus geometry. Systems with four and six fermions are accessible

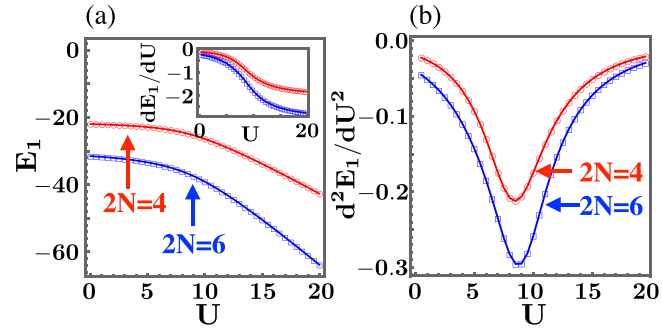

FIG. 8. (a) Ground state energy E_1 at $(n_\uparrow, n_\downarrow; \frac{n_\uparrow n_\downarrow}{n_\uparrow + n_\downarrow}) = (1, 1; 1/2)$ on a 1-icosahedron. The results in red and blue are for the systems considered in Figs. 5(a) and 5(b), respectively. The inset shows the first derivative dE_1/dU. (b) Second derivative d^2E_1/dU^2.

to our study. In the spherical geometry, we find that the (1,1) fermionic state adiabatically evolves into the 1/2 bosonic state. In the torus geometry, we find that the (1,1), (1,2), and (1,3) fermionic states merge into degenerate multiplets of the 1/2, 2/3, and 3/4 bosonic FQHE ground states. In contrast, there is no adiabatic continuity for the excited states. This observation—namely that the nature of excitations changes while the ground state evolves adiabatically—resembles the relation between the $\nu = 2/5$ Jain state and the Gaffnian state [39,40] or the BCS to BEC crossover.

It is evident that the crossover from (1,1) to 1/2 state takes place at approximately $U \approx 10$. In Fig. 5, the energy gap separating the ground state and the first excited state changes its behavior qualitatively at $U \approx 10$. In the torus geometry, the ground state goes from a nondegenerate state to a nearly degenerate doublet at $U \approx 10$. Reference [34] has identified a transition at this value by a consideration of the entanglement spectrum. Finally, Fig. 8 shows the ground state energy E_1, the first derivative dE_1/dU (in the inset), and the second derivative d^2E_1/dU^2. While E_1 is a continuous function of U, $-d^2E_1/dU^2$ has a peak at $U \approx 10$, which becomes sharper as the particle number increases. Following the work of Wu *et al.* [35], this suggests a continuous phase transition in the thermodynamic limit.

Our work can be generalized in many directions. An immediate extension involves examining the adiabatic continuity between the $\nu = 1$ IQHE states of three species of fermionic partons and the $\nu = 1/3$ FQHE state of fermions. This can be demonstrated using a generalized Hubbard model of spin-1 fermions, which incorporates the onsite attractive interaction, $-U$, and the nearest-neighbor repulsive interaction, V. Under appropriate conditions, the system exhibits the IQHE state at $U = V = 0$ while the $\nu = 1/3$ FQHE state at $U \to \infty$ and $V > 0$.

It is also natural to ask how the edge states of the IQHE evolve into those of the FQHE in our adiabatic scheme. This may in principle be accomplished either by creating a confinement potential on the sphere or by evaluating the entanglement spectrum of the uniform ground state. Unfortunately, the system sizes required for a meaningful study of the edge states are too large for our exact diagonalization calculation.

Mean field theory [62] has suggested emergence of superconducting states in the Hubbard model with a magnetic field. A numerical investigation allowing for a competition between the FQHE and the superconducting states is left for a future study.

ACKNOWLEDGMENTS

We thank Yinghai Wu, G. J. Sreejith and A. C. Balram for helpful discussions, and we are especially grateful to Yinghai Wu for bringing to our attention previous work along this direction. K.K. acknowledges financial support from JSPS Overseas Research Fellowships. K.K. was supported in part by JSPS KAKENHI Grant No. JP23K19036 and JST CREST Grant No. JPMJCR18T2. At The Pennsylvania State University, the part relating to pairing in the presence of a magnetic field induced by attractive interaction was supported by U.S. Department of Energy, Office of Basic Energy Sciences, under Grant No. DE-SC-0005042 (J.S. and J.K.J), and the part relating to exact models by the U.S. National Science Foundation under Grant No. DMR-2037990 (J.K.J.). J.S. was supported by the U.S. Department of Energy, Office of Basic Energy Sciences under Award No. DE-SC0022245 at William & Mary. We acknowledge Advanced CyberInfrastructure computational resources provided by The Institute for CyberScience at The Pennsylvania State University and the computational resources offered by Research Institute for Information Technology, Kyushu University.

APPENDIX: EFFECTIVE HAMILTONIAN

In this section, we derive the effective Hamiltonian $H_{\rm eff}$ in Eq. (9) using the degenerate perturbation theory. Let us rewrite the Hamiltonian in Eq. (7) as $H = H_{\rm kin} + H_{\rm int}$ with

$$H_{\rm kin} = -t \sum_{\langle ij \rangle} \sum_{\sigma=\uparrow,\downarrow} \hat{c}^\dagger_{i\sigma} e^{i\alpha_{ij\sigma}} \hat{c}_{j\sigma}, \tag{A1}$$

$$H_{\rm int} = -U \sum_i \hat{n}_{i\uparrow}\hat{n}_{i\downarrow}. \tag{A2}$$

At $t/U = 0$, the ground state is macroscopically degenerate, where all sites are either doubly occupied or empty. This degeneracy is lifted by the second order perturbation: $H_{\rm eff} = PH_{\rm kin}Q\frac{1}{E_0 - H_{\rm int}}QH_{\rm kin}P$, where P is the ground state subspace of $H_{\rm int}$, $H_{\rm int}P = E_0 P$, and $Q = 1 - P$. Since there are two $H'_{\rm kin}$s in $H_{\rm eff}$, it is enough to consider the two-site problem to get the expression. We have

$$\begin{aligned} H_{\rm eff}[\hat{c}^\dagger_{1\uparrow}\hat{c}^\dagger_{1\downarrow}|0\rangle] &= PH_{\rm kin}Q\frac{1}{E_0 - H_{\rm int}}QH_{\rm kin}P[\hat{c}^\dagger_{1\uparrow}\hat{c}^\dagger_{1\downarrow}|0\rangle] \\ &= PH_{\rm kin}\frac{t}{U}(e^{i\alpha_{21\uparrow}}\hat{c}^\dagger_{2\uparrow}\hat{c}^\dagger_{1\downarrow} + e^{i\alpha_{21\downarrow}}\hat{c}^\dagger_{1\uparrow}\hat{c}^\dagger_{2\downarrow})|0\rangle \\ &= \frac{-2t^2}{U}(e^{i(\alpha_{21\uparrow}+\alpha_{21\downarrow})}\hat{c}^\dagger_{2\uparrow}\hat{c}^\dagger_{2\downarrow} + \hat{c}^\dagger_{1\uparrow}\hat{c}^\dagger_{1\downarrow})|0\rangle, \end{aligned} \tag{A3}$$

$$H_{\rm eff}[\hat{c}^\dagger_{2\uparrow}\hat{c}^\dagger_{2\downarrow}|0\rangle] = \frac{-2t^2}{U}(e^{i(\alpha_{12\uparrow}+\alpha_{12\downarrow})}\hat{c}^\dagger_{1\uparrow}\hat{c}^\dagger_{1\downarrow} + \hat{c}^\dagger_{2\uparrow}\hat{c}^\dagger_{2\downarrow})|0\rangle, \tag{A4}$$

$$H_{\rm eff}|0\rangle = 0, \tag{A5}$$

$$H_{\rm eff}[\hat{c}^\dagger_{1\uparrow}\hat{c}^\dagger_{1\downarrow}\hat{c}^\dagger_{2\uparrow}\hat{c}^\dagger_{2\downarrow}]|0\rangle = 0. \tag{A6}$$

Within the subspace P, $\hat{c}^\dagger_{i\uparrow}\hat{c}^\dagger_{i\downarrow}$ obeys the commutation relation:

$$P[\hat{c}^\dagger_{i\uparrow}\hat{c}^\dagger_{i\downarrow}, \hat{c}_{j\uparrow}\hat{c}_{j\downarrow}]P = P(1 - (\hat{n}_{i\uparrow} - \hat{n}_{i\downarrow}))\delta_{ij}P = \delta_{ij}. \tag{A7}$$

Replacing $\hat{c}^\dagger_{i\uparrow}\hat{c}^\dagger_{i\downarrow}$ with a bosonic operator $\hat{b}^\dagger_i$, we rewrite Eqs. (A3)–(A6) as

$$H_{\rm eff}\hat{b}^\dagger_1|0\rangle = -\beta(e^{i(\alpha_{21\uparrow}+\alpha_{21\downarrow})}\hat{b}^\dagger_2|0\rangle + \hat{b}^\dagger_1|0\rangle), \tag{A8}$$

$$H_{\rm eff}\hat{b}^\dagger_2|0\rangle = -\beta(e^{i(\alpha_{12\uparrow}+\alpha_{12\downarrow})}\hat{b}^\dagger_1|0\rangle + \hat{b}^\dagger_2|0\rangle), \tag{A9}$$

$$H_{\rm eff}|0\rangle = 0, \tag{A10}$$

$$H_{\rm eff}\hat{b}^\dagger_1\hat{b}^\dagger_2|0\rangle = 0, \tag{A11}$$

where $\beta = 2t^2/U$. Here, bosons created by $\hat{b}^\dagger_i$'s are hard-core due to $\hat{b}^2_i = (\hat{c}^\dagger_{i\uparrow}\hat{c}^\dagger_{i\downarrow})^2 = 0$. The relations in Eqs. (A8)–(A11) are satisfied by the following expression:

$$H_{\rm eff} = -\beta(e^{i(\alpha_{21\uparrow}+\alpha_{21\downarrow})}\hat{b}^\dagger_2\hat{b}_1 + \text{H.c.}) - \beta(\hat{n}_1 + \hat{n}_2) + 2\beta\hat{n}_1\hat{n}_2, \tag{A12}$$

where $\hat{n}_i = \hat{b}^\dagger_i\hat{b}_i$. The expression for a similar problem in Ref. [63] lacks the last term. By summing up $H_{\rm eff}$ in Eq. (A12) over all bonds for a given system, one obtains the general form shown in Eq. (9).

[1] K. V. Klitzing, G. Dorda, and M. Pepper, Phys. Rev. Lett. **45**, 494 (1980).
[2] D. C. Tsui, H. L. Stormer, and A. C. Gossard, Phys. Rev. Lett. **48**, 1559 (1982).
[3] D. J. Thouless, M. Kohmoto, M. P. Nightingale, and M. den Nijs, Phys. Rev. Lett. **49**, 405 (1982).
[4] M. Kohmoto, Ann. Phys. **160**, 343 (1985).
[5] Q. Niu, D. J. Thouless, and Y.-S. Wu, Phys. Rev. B **31**, 3372 (1985).
[6] R. B. Laughlin, Phys. Rev. Lett. **50**, 1395 (1983).
[7] F. D. M. Haldane, Phys. Rev. Lett. **51**, 605 (1983).
[8] B. I. Halperin, Phys. Rev. Lett. **52**, 1583 (1984).
[9] D. Arovas, J. R. Schrieffer, and F. Wilczek, Phys. Rev. Lett. **53**, 722 (1984).
[10] J. K. Jain, Phys. Rev. Lett. **63**, 199 (1989).
[11] J. K. Jain, *Composite Fermions* (Cambridge University Press, New York, 2007).
[12] M. Greiter and F. Wilczek, Mod. Phys. Lett. B **04**, 1063 (1990).
[13] M. Greiter and F. Wilczek, Nucl. Phys. B **370**, 577 (1992).
[14] K. Kudo and Y. Hatsugai, Phys. Rev. B **102**, 125108 (2020).
[15] S. Pu and J. K. Jain, Phys. Rev. B **104**, 115135 (2021).
[16] K. Kudo, Y. Kuno, and Y. Hatsugai, Phys. Rev. B **104**, L241113 (2021).
[17] M. Greiter and F. Wilczek, Phys. Rev. B **104**, L121111 (2021).

[18] T. Hansson and S. Kivelson, in *FRANK WILCZEK: 50 Years of Theoretical Physics* (World Scientific, Singapore, 2022), pp. 103–123.
[19] K. Kudo and Y. Hatsugai, Phys. Rev. B **106**, 075120 (2022).
[20] J. K. Jain, Phys. Rev. B **40**, 8079 (1989).
[21] J. K. Jain, Phys. Rev. B **41**, 7653 (1990).
[22] X. G. Wen, Phys. Rev. Lett. **66**, 802 (1991).
[23] A. C. Balram, M. Barkeshli, and M. S. Rudner, Phys. Rev. B **98**, 035127 (2018).
[24] A. C. Balram, S. Mukherjee, K. Park, M. Barkeshli, M. S. Rudner, and J. K. Jain, Phys. Rev. Lett. **121**, 186601 (2018).
[25] A. C. Balram, M. Barkeshli, and M. S. Rudner, Phys. Rev. B **99**, 241108(R) (2019).
[26] Y. Wu, T. Shi, and J. K. Jain, Nano Lett. **17**, 4643 (2017).
[27] Y. Kim, A. C. Balram, T. Taniguchi, K. Watanabe, J. K. Jain, and J. H. Smet, Nat. Phys. **15**, 154 (2019).
[28] W. N. Faugno, A. C. Balram, M. Barkeshli, and J. K. Jain, Phys. Rev. Lett. **123**, 016802 (2019).
[29] W. N. Faugno, J. K. Jain, and A. C. Balram, Phys. Rev. Res. **2**, 033223 (2020).
[30] A. C. Balram, J. K. Jain, and M. Barkeshli, Phys. Rev. Res. **2**, 013349 (2020).
[31] A. C. Balram and A. Wójs, Phys. Rev. Res. **2**, 032035(R) (2020).
[32] K. Yang and H. Zhai, Phys. Rev. Lett. **100**, 030404 (2008).
[33] T.-L. Ho, arXiv:1608.00074.
[34] C. Repellin, T. Yefsah, and A. Sterdyniak, Phys. Rev. B **96**, 161111(R) (2017).
[35] Y.-H. Wu, H.-H. Tu, and M. Cheng, Phys. Rev. Lett. **131**, 256502 (2023).
[36] B. Paredes, P. Fedichev, J. I. Cirac, and P. Zoller, Phys. Rev. Lett. **87**, 010402 (2001).
[37] Y. Zhang, G. J. Sreejith, N. D. Gemelke, and J. K. Jain, Phys. Rev. Lett. **113**, 160404 (2014).
[38] S. H. Simon, E. H. Rezayi, N. R. Cooper, and I. Berdnikov, Phys. Rev. B **75**, 075317 (2007).
[39] C. Tőke and J. K. Jain, Phys. Rev. B **80**, 205301 (2009).
[40] B. Yang, Y.-H. Wu, and Z. Papić, Phys. Rev. B **100**, 245303 (2019).
[41] T. Einarsson, Phys. Rev. Lett. **64**, 1995 (1990).
[42] X. G. Wen, E. Dagotto, and E. Fradkin, Phys. Rev. B **42**, 6110 (1990).
[43] J. Léonard, S. Kim, J. Kwan, P. Segura, F. Grusdt, C. Repellin, N. Goldman, and M. Greiner, Nature (London) **619**, 495 (2023).
[44] A. J. Leggett, in *Modern Trends in the Theory of Condensed Matter*, edited by A. Pekalski and R. Przystaw (Springer, Berlin, 1980).
[45] M. Randeria and E. Taylor, Annu. Rev. Condens. Matter Phys. **5**, 209 (2014).
[46] C. A. Regal, M. Greiner, and D. S. Jin, Phys. Rev. Lett. **92**, 040403 (2004).
[47] M. Bartenstein, A. Altmeyer, S. Riedl, S. Jochim, C. Chin, J. H. Denschlag, and R. Grimm, Phys. Rev. Lett. **92**, 120401 (2004).
[48] M. W. Zwierlein, C. A. Stan, C. H. Schunck, S. M. F. Raupach, A. J. Kerman, and W. Ketterle, Phys. Rev. Lett. **92**, 120403 (2004).
[49] W. Wu, C. Kallin, and A. Brass, Phys. Rev. B **42**, 2222 (1990).
[50] M. Ö. Oktel, The European Physical Journal D **66**, 88 (2012).
[51] B. Jowett, in *The Dialogues of Plato* (Scribner, Armstrong, 1873), Vol. 3.
[52] A. Šiber, Symmetry **12**, 556 (2020).
[53] Y. Hatsugai, K. Ishibashi, and Y. Morita, Phys. Rev. Lett. **83**, 2246 (1999).
[54] In our algorithm, the Lanczos iteration terminates when the lowest eigenvalue $E_g(i)$ at ith step satisfies $|E_g(i) - E_g(i-M)| < 10^{-\epsilon}$. For example, we set $M = 3$ and $\epsilon = 8$ in Fig. 5(a). This criterion allows us to identify the lowest energy even if the ground state has degeneracy. The nth lowest energy is computed as the "lowest energy" of a matrix where the lowest (or degenerate) $n-1$ energy states are energetically shifted using their eigenvectors.
[55] G. Dev and J. K. Jain, Phys. Rev. Lett. **69**, 2843 (1992).
[56] T. Fukui, Y. Hatsugai, and H. Suzuki, J. Phys. Soc. Jpn. **74**, 1674 (2005).
[57] H. Watanabe, Phys. Rev. B **98**, 155137 (2018).
[58] M. B. Hastings and S. Michalakis, Commun. Math. Phys. **334**, 433 (2015).
[59] T. Koma, arXiv:1504.01243.
[60] S. Bachmann, A. Bols, W. De Roeck, and M. Fraas, Ann. Henri Poincaré **19**, 695 (2018).
[61] K. Kudo, H. Watanabe, T. Kariyado, and Y. Hatsugai, Phys. Rev. Lett. **122**, 146601 (2019).
[62] J. Schirmer, J. K. Jain, and C. X. Liu (unpublished).
[63] K. Kudo and J. Schirmer, Phys. Rev. B **106**, 214517 (2022).

Correction: Missing information from the fourth sentence of the Acknowledgments has been inserted.